Inductive measurement of the free surface of liquid metals

Zürner, T.; Ratajczak, M.; Wondrak, T.; Eckert, S.;

Originally published:

October 2017

Measurement Science and Technology 28(2017)11, 115301

DOI: https://doi.org/10.1088/1361-6501/aa7f58

Perma-Link to Publication Repository of HZDR:

https://www.hzdr.de/publications/Publ-25295

Inductive detection of the free surface of liquid metals

Till Zürner,[1, 2, *] Matthias Ratajczak,[1] Thomas Wondrak,[1] and Sven Eckert[1]

[1] *Helmholtz-Zentrum Dresden - Rossendorf, Institute of Fluid Dynamics, Department of Magnetohydrodynamics, Bautzner Landstraße 400, 01328 Dresden, Germany*

[2] *Technische Universität Dresden, School of Science, Department of Physics*

(Dated: February 23, 2017)

A novel measurement system to determine the surface position and topology of liquid metals is presented. It is based on the induction of eddy currents by a time-harmonic magnetic field and the subsequent measurement of the resulting secondary magnetic field using gradiometric induction coils. The system is validated experimentally for static and dynamic surfaces of the low-melting liquid metal alloy gallium-indium-tin in a narrow vessel. It is shown that a precision below 1 mm and a time resolution of at least 20 Hz can be achieved.

Keywords: Inductive measurement, liquid metal, surface topology

I. INTRODUCTION

Monitoring process parameters in industrial production is indispensable to improve the quality and quantity of the resulting products. If liquids with free surfaces are involved, important parameters are the surface position and shape. There are already several systems commercially available to determine these properties. Ultrasonic transducers emit a sound pulse, record the echo from the surface and calculate the liquid level from the time difference between emission and reception of the ultrasound wave. Optical systems project a laser point or line on the surface and record the position of the projection with a camera from the side.

For electrically conducting liquids such as metal melts it is possible to utilize the induction of eddy currents and the subsequent measurement of the resulting magnetic field. Commercial sensors based on this principle exist and are used for level measurement in aluminium [1] and steel [2]. Khalilov et. al. [3] devised an inductive system to measure the position and height of a layer of magnesium in the production of titanium.

Aside from the last example these systems are positioned above the surface of the liquid and require free space in between. This is not always possible for closed vessels and since metal melts are often very hot, the sensors are subjected to high temperatures and may require cooling. The system by Kalilov et. al. circumvents these issues, is however build for one specific vessel geometry. The non-inductive measurement methods mentioned above also have the disadvantage, that they cannot measure the fluid surface accurately in realistic situations, when a layer of slag is present on top of the surface.

In this paper we present an inductive measurement system that aims to be applicable for open and closed containers of arbitrary geometry. The concept consists in the configuration of several specially designed sensors at different positions around the vessel to measure the surface level locally. Such a setup provides a rough surface level distribution across the vessel. This process is comparable to the method of magnetic induction tomography (MIT), where multiple inductive sensors are arranged around a test volume and their cross-signals are evaluated by solving an inverse problem. However, to ease the analysis of the measurement data, level measurements in our system will be done by an individual calibration of each sensor.

In the following section II a brief summary of the theory of the induction of eddy currents and of the measurement principles is given. The algorithm to reconstruct the free surface presented in section III is based on finite-element-method (FEM) simulations using the software *Opera-3d*. This design is then validated experimentally for the case static surfaces in section IV and for capturing the dynamics of temporally variable surfaces in section V.

II. THEORY

We consider a liquid metal with constant electric conductivity σ in the region V_σ embedded in a non-conducting surrounding (see Figure 1). Consequently, there is a jump in the conductivity from zero to σ on the surface of the liquid $S_\sigma = \partial V_\sigma$. The magnetic excitation field $\boldsymbol{B}_0$ is generated by a coil outside V_σ with a time-harmonic current density $\tilde{\boldsymbol{J}}_0(\boldsymbol{r}, t) = \boldsymbol{J}_0(\boldsymbol{r}) e^{i\omega t}$ of angular frequency ω, where $\boldsymbol{J}_0(\boldsymbol{r}) \in \mathbb{R}^3$. Assuming linear material characteristics all other time-dependent quantities derived from this excitation are time-harmonic with the same frequency, but can experience a phase shift. As a result an arbitrary quantity $\tilde{Q}(\boldsymbol{r}, t)$ (scalar or vector) can be fully described by a complex time-independent value $Q(\boldsymbol{r})$

$$\begin{aligned} \tilde{Q}(\boldsymbol{r}, t) = Q(\boldsymbol{r})\, e^{i\omega t} &= \left[|Q|(\boldsymbol{r}) e^{i\phi(\boldsymbol{r})} \right] e^{i\omega t} \\ &= \left[Q_R(\boldsymbol{r}) + i Q_I(\boldsymbol{r}) \right] e^{i\omega t}. \end{aligned} \tag{1}$$

Here $|Q|$ is the amplitude of the complex quantity and ϕ its phase shift towards $\boldsymbol{J}_0$. An alternative representation consists of the real part Q_R that is in phase with $\boldsymbol{J}_0$

* Corresponding author: t.zuerner@hzdr.de

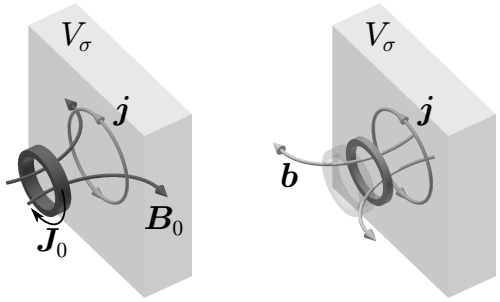

(a) (b)

Figure 1. Schematic view of the measurement principle: (a) Induction of eddy currents $\boldsymbol{j}$ in the fluid by the time-harmonic magnetic field $\boldsymbol{B}_0$ produced by the electric current $\boldsymbol{J}_0$ in the excitation coil. (b) Measurement of the secondary magnetic field $\boldsymbol{b}$ produced by $\boldsymbol{j}$ in the detector coil.

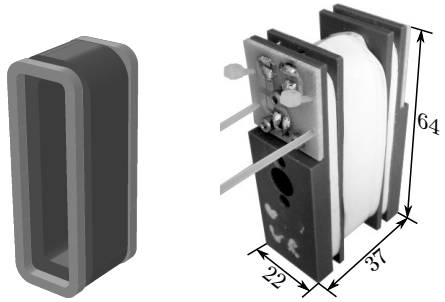

(a) (b)

Figure 2. (a) Schematic view of the coil windings and (b) photo of the manufactured sensor with dimensions in mm. The excitation coil is in dark grey, and the detector coils are in light grey.

(in-phase signal) and the imaginary part Q_I that is in opposition to $\boldsymbol{J}_0$ (out-phase signal).

The induction of eddy currents $\boldsymbol{j}$ into liquid metals (Figure 1(a)) is governed by Maxwell's equations in quasistatic approximation and Ohm's law [4].

$$\begin{aligned} \boldsymbol{\nabla}\cdot\boldsymbol{E} &= \frac{\rho_e}{\varepsilon_0}\,, \quad & \boldsymbol{\nabla}\times\boldsymbol{E} &= -i\omega\boldsymbol{B} \\ \boldsymbol{\nabla}\cdot\boldsymbol{B} &= 0\,, & \boldsymbol{\nabla}\times\boldsymbol{B} &= \mu_0(\boldsymbol{J}_0+\boldsymbol{j}) \end{aligned} \tag{2}$$

$$\boldsymbol{j} = \sigma\boldsymbol{E} \tag{3}$$

Here $\boldsymbol{E}$ and $\boldsymbol{B}$ are the electric and magnetic field, ε_0 and μ_0 are the electric permittivity and magnetic permeability of free space and ρ_e the electric charge density. Any effects of the fluid velocity on the magnetic field are neglected. For a given excitation current density $\boldsymbol{J}_0$, frequency ω and electric conductivity σ the only remaining degree of freedom is the shape of the conducting region V_σ. The effect of the time-variation of the excitation is characterized by the shielding parameter $R_\omega = \mu_0\sigma\omega l^2$. For high $R_\omega \gg 1$ the skin effect, which expels the magnetic field from the inside of the conductor, has to be taken into account. For low $R_\omega \ll 1$ we can set $\boldsymbol{\nabla}\times\boldsymbol{E} = -i\omega\boldsymbol{B}_0$ in (2).

The resulting magnetic field $\boldsymbol{B}$, consisting of the excitation field $\boldsymbol{B}_0$ and the induced secondary field $\boldsymbol{b}$, is measured by induction coils (Figure 1(b)). The voltage U_M induced in an induction coil is

$$U_M = -i\omega\int_{S_M}\boldsymbol{B}\cdot\boldsymbol{n}\,\mathrm{d}S\,, \tag{4}$$

where S_M is the surface enclosed by the wire of the coil with a normal vector $\boldsymbol{n}$. The prefactor $-i = \exp(-i\pi/2)$ represents a phase shift of $-\pi/2 = -90°$. As a result the contribution of the in-phase (out-phase) part of the magnetic field gets shifted into the out-phase (in-phase) part of the voltage.

The following section will outline the design of the measurement system based on these theoretical considerations.

III. SENSOR-DESIGN

The sensor consists of an excitation coil and two detector coils. The excitation coil is operated by a time-harmonic current $\boldsymbol{J}_0$, which generates the excitation field $\boldsymbol{B}_0$. The time-variation of the magnetic field enables us to use detector coils to measure the resulting magnetic field.

The excitation and detector coils are build as rectangular coils. The magnetic field of such a coil is strongest along its symmetry axis. Consequently, the axis of the excitation coil, which is situated next to the container, is chosen to point towards the liquid metal. Owing to Lenz's law we can expect the induced field $\boldsymbol{b}$ to be primarily anti-parallel to the excitation field. To maximize the induced voltage in the detector coil by $\boldsymbol{b}$, it will be aligned with the expected direction of the induced field, which is parallel to the axis of the excitation coil. The location of the detector coil is between the excitation coil and the fluid container to be as close as possible to the eddy currents to be measured. This placement however also results in a voltage induced by $\boldsymbol{B}_0$ that is generally much larger than the signal created by $\boldsymbol{b}$. To subtract this undesired background a second detector coil identical to the first one is placed at the back of the excitation coil. If the two detector coils are exactly symmetric with respect to the excitation coil, $\boldsymbol{B}_0$ induces the same voltage in both coils. Consequently, if the detector coils are connected to form a gradiometric coil, these voltages cancel each other and the background signal vanishes. The first detector coil will be referred to as front coil, the second one as back coil.

A coaxial alignment of the coils allows them to be wound on a joint body. This simplifies manufacturing and prevents position changes of the coils relative to each other, which is important during operation to provide a stable signal.

The measurement system will be tested at a narrow rectangular container (see sections IV and V). Because of this geometry the most relevant changes of the sur-

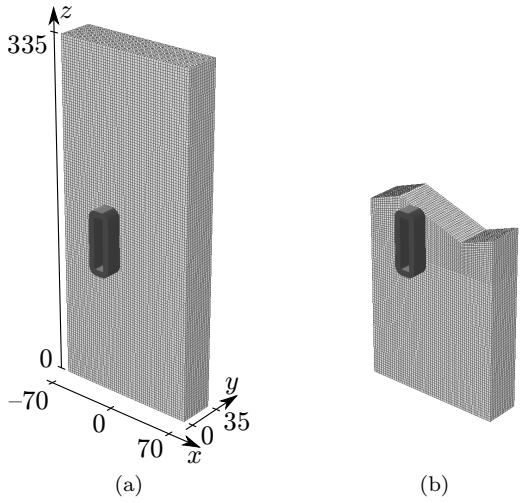

Figure 3. Simulation geometry for (a) a plane surface (dimensions in mm) and (b) a zick-zack surface profile. The excitation coil is displayed in dark grey.

face shape can be expected to appear in the direction of the wide face of the vessel. We choose five measurement points along the wide face as a compromise between sensor width and resolution of the surface shape.

The final geometry of the coils is displayed in Figure 2(a) and 2(b). The coil parameters were determined to maximize the measured signal while considering restrictions of the manufacturing process and of the size of the sensor for easier handling. To accomplish this final sensor design, parameter studies were performed through FEM simulations.

A. Surface Level Simulations

The simulations were done using the program *Opera-3d* by *Cobham CTS Limited*. Its *Elektra Steady-State* solver considers equations (2) and (3) in a potential formulation. The fluid volume V_σ was modelled by a cuboid of width 140 mm, depth 35 mm and a variable height from 5 mm to 335 mm, representing different surface levels (see Figure 3(a)). The conductivity of the volume was set to $\sigma = 3.29 \times 10^6\,\mathrm{S/m}$, which is the value of the fluid used in the experimental validation in sections IV and V. The sensor is placed in the centre of the wide face of the container at $x = 0\,\mathrm{mm}$ and $z = 335\,\mathrm{mm}/2 = 167.5\,\mathrm{mm}$. The sensor position is given by its geometric centre. The simulation results for a frequency of 50 Hz are displayed in Figure 4.

At surface levels far below the sensor there is no background signal ($|U_M|, U_{M,R}, U_{M,I} \simeq 0$ in Figure 4), since the gradiometric coil cancels out the excitation field $\boldsymbol{B}_0$ and the induced currents in the distant volume V_σ are too weak to generate a significant signal. The accompanying phase ϕ_M is $-90°$. Since $\boldsymbol{B}_0$ is in phase with the excitation current, this phase shift originates from the induction process in the detection coils as mentioned in (4).

With increasing level all components of the signal, except its phase, follow a similar curve: When the surface level passes the sensor, the components increase or decrease from their background value until they reach a constant saturation value at high surface levels. This transition between the two constants follows the shape of a sigmoid function

$$q(h) = \frac{\Delta q}{1 + \exp\left(\frac{h - h_0}{\Delta h}\right)} + q_0\,, \tag{5}$$

where q is the measured component and h the surface level. The fit-parameters of the function are the background signal q_0, the difference of background and saturation value Δq, the z-position h_0 of the transition and its width Δh. In Figure 7 the function (5) is fitted to the measured data. The change in the signal Δq is tens of degrees in case of the phase and in the range of several mV for the other components, which can be measured easily. The curves show that with this sensor it is possible to measure the surface level in a range of 60 to 70 mm. This dynamic range is not symmetric with respect to the sensor, but rather lies about 10 to 20 mm above the centre of the sensor at $z = 167.5\,\mathrm{mm}$.

Only the phase shift (Figure 4(d)) of the signal does not follow a sigmoid curve. Before saturating it reaches a maximum value when the surface level is at the same height as the centre of the sensor. As a result the phase-surface level relation is not bijective and thus ambiguous, which makes it unfit for determining the surface level directly.

Once the fit-parameters are known, the inversion of (5) can be used as a model to determine the surface level:

$$h(q) = h_0 + \Delta h \cdot \ln\left(\frac{\Delta q}{q - q_0} - 1\right). \tag{6}$$

It is important to note that in this model the parameters h_0, Δh, q_0 and Δq are dependent on the vessel geometry, sensor position, excitation characteristics (ω and $|\boldsymbol{J}_0|$) and the fluid properties (σ).

B. Surface Topology Reconstruction

As already mentioned in the introduction, we want to use the sensor to measure the local surface level at different positions along the container. To test this approach an FEM-simulation with a prescribed static surface shape was conducted. The chosen shape is a zick-zack line $H(x)$ along the wide face (x-axis) which approximates an asymmetric standing wave (see Figure 3(b)). Along the y-axis the surface height was kept constant. A sine curve could have been used as well, but the chosen shape has the same general features and was also used during experimental validation (section IV C), where it

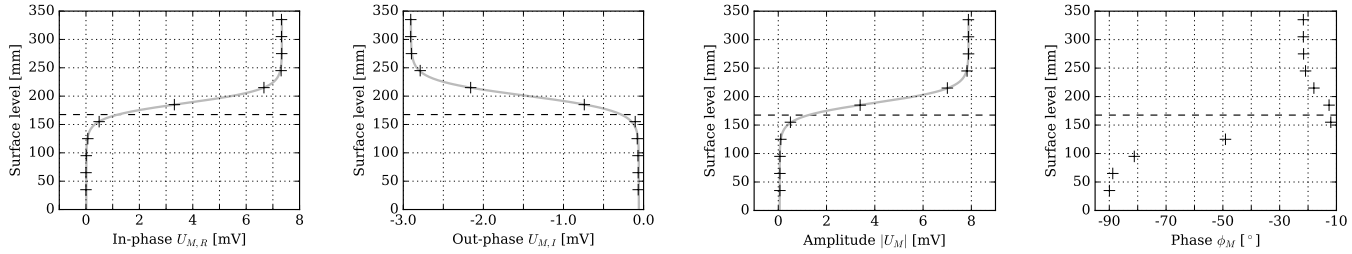

Figure 4. Components of the simulated voltage U_M for different fill heights: (a) In-phase signal $U_{M,R}$, (b) out-phase signal $U_{M,I}$, (c) amplitude $|U_M|$ and (d) phase ϕ_M. The black crosses are the simulated data, the solid grey lines are the fits of function (5) to the data and the dashed black line shows the vertical sensor position.

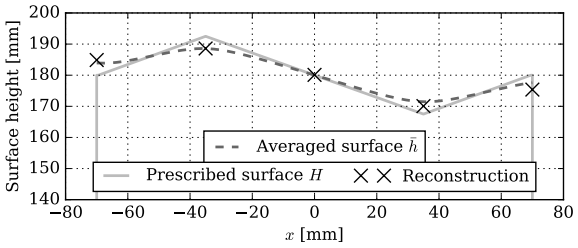

Figure 5. Result of the surface topology reconstruction from simulations using the model function (6), fitted to $U_{M,R}$. $\bar{h}$ was calculated using the wall thickness $d = 8\,\text{mm}$ in (8).

was easier to construct. The shape amplitude was exaggerated to increase the response of the sensor; in reality much smaller wave amplitudes are expected.

The mean height of the surface was adjusted to be at the same height as the sensor. The sensor was simulated at five positions along the wide face: $x = -70, -35, 0, 35, 70\,\text{mm}$. The in-phase signal $U_{M,R}$ was then converted into a local surface level using the model (6) with the corresponding parameters, which are calculated for each position according to section III A.

The resulting reconstructed local surface levels are shown in Figure 5 as black crosses. The reconstruction does not exactly match the prescribed shape but rather represents a mean surface level of the surrounding area. As a result the amplitude of the shape is smaller than the target value. On the edges the level is over- or underestimated depending on whether the surface ascends or descends in the surrounding. Only in the middle of the wide face ($x = 0\,\text{mm}$) does the reconstruction match the predefined surface level, since the mean surface level in its vicinity is equal to the prescribed one.

To show that this deviation of the reconstruction is an intrinsic property of the inductive measurement method we consider the law of Biot-Savart:

$$\boldsymbol{b}(\boldsymbol{r}) = \frac{\mu_0}{4\pi} \int_{V_\sigma} \frac{\boldsymbol{j}(\boldsymbol{r}') \times (\boldsymbol{r} - \boldsymbol{r}')}{\|\boldsymbol{r} - \boldsymbol{r}'\|^3} \,\mathrm{d}V' \,. \tag{7}$$

$\|\cdot\|$ denotes the Euclidean norm of a vector. The induced field $\boldsymbol{b}$ at the sensor position $\boldsymbol{r}$ is comprised of all eddy currents $\boldsymbol{j}$ in the fluid volume V_σ. Aside from the cross product this integral can be seen as an average of all eddy currents weighted by their inverse square distance to the sensor, which resembles a convolution $\boldsymbol{j}(\boldsymbol{r}) * \|\boldsymbol{r}\|^{-2}$. To demonstrate this behaviour the prescribed surface shape $H(x)$ is convoluted with $W(x) = 1/(x^2 + d^2)$, which represents the $\|\boldsymbol{r}\|^{-2}$ "convolution" kernel with d being the distance of the sensor to the melt in y-direction. Any additional y- and z-dependences of $\|\boldsymbol{r}\|$ are neglected for the sake of simplicity. The resulting averaged surface shape $\bar{h}(x)$ is

$$\bar{h}(x) = \frac{1}{N(x)} \int_{x_l}^{x_r} H(x')\, W(x - x') \,\mathrm{d}x' \,, \tag{8}$$

$$N(x) = \frac{1}{d} \left[\arctan\left(\frac{x_r - x}{d}\right) - \arctan\left(\frac{x_l - x}{d}\right) \right] . \tag{9}$$

The factor $N(x)$ was introduced to normalize $W(x - x')$ on the interval $x' \in [x_l, x_r]$ for fixed x. Here $x_l = -70\,\text{mm}$ and $x_r = 70\,\text{mm}$ are the position of the left and right edge of the wide face. For d the wall-thickness of 8 mm is chosen, i.e. the distance between the fluid and the sensor. The resulting curve $\bar{h}(x)$ is plotted as a dashed line in Figure 5. We see that it closely resembles the points reconstructed by the simulation. This shows that the sensor produces a weighted average of the surrounding surface level with an inverse square distance weight function. Despite this discrepancy the simulation result correctly represents the overall surface shape and important topological properties such as symmetries. If applied to real surfaces this effect is also expected to be less prominent, since hard edges as in this example do not appear and surface waves are much smoother.

IV. EXPERIMENTAL VALIDATION: STATIC SURFACE

For validating the simulations shown in section III a prototype of the sensor was built (see Figure 2(b)). In this section we will concentrate on experiments with static surfaces as used in the simulations.

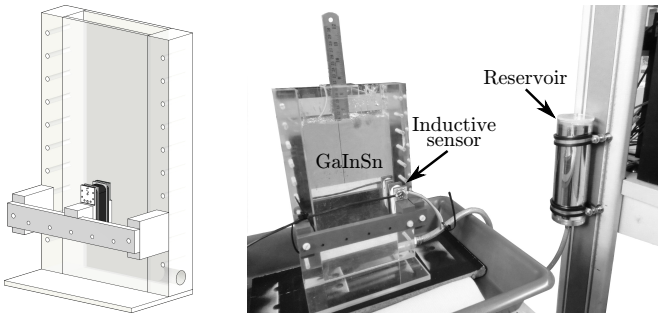

(a) (b)

Figure 6. (a) Schematic sketch and (b) photo of the experimental setup.

A. Setup

To match the geometry of the simulation a rectangular vessel of inner height 335 mm, inner width 140 mm, inner depth 35 mm and wall thickness 8 mm is used (see Figure 6). The vessel is filled with the alloy gallium-indium-tin (GaInSn [5]), which is liquid at room temperature and has an electric conductivity of 3.29×10^6 S/m at 20 °C [6]. To change the surface level in the vessel, a reservoir is connected to its base by a hose. Raising or lowering this reservoir allows the variation of the amount of fluid in the vessel.

The alternating excitation current is supplied by a *Kepco* power supply (*BOP 20-50GL*) and measured by a *LEM IT 60-S* current transformer. All signals are recorded by a 24-bit analogue-digital-converter (*LTT24* by *LTT Labortechnik Tasler GmbH*) as transient signals (sampling frequency 5 kHz) and demodulated into amplitude and phase using the Lomb-Scargle algorithm [7].

B. Surface Level Measurement

In order to examine the relationship between the surface level and the induced signal the first experiments are conducted with a plain surface. The sensor is placed in the middle of the wide face of the vessel at a height of 130 mm. The excitation coil is operated by a 60 Hz alternating current of 1 A. We chose this frequency to avoid interference from the ubiquitous fields of the 50 Hz power grid. The surface level is changed incrementally and the resulting voltages U_M of the gradient coil are recorded (see Figure 7).

Like in the simulations (Figure 4) amplitude, in- and out-phase signal of the induced voltage follow the curve of a sigmoid. The phase signal shows the local maximum that was present in the simulations, albeit less pronounced. This difference results from slight asymmetries of the gradiometric coil, which are responsible that the voltages induced by $\boldsymbol{B}_0$ do not cancel each other completely. This remaining voltage of 14.0 mV can be seen in the amplitude and the out-phase signal for low surface levels (Figures 7(c) and 7(b)). Measuring the voltage that is induced by $\boldsymbol{B}_0$ into the front coil alone results in an amplitude of 808.0 mV. This means, that the gradient coil reduces the background signal of $\boldsymbol{B}_0$ by two orders of magnitude.

Aside from this difference the experimental results closely match the simulations. Thus it is possible to use the same calibration procedure as for the simulations. Just like in section III the in-phase signal will be used for calibration.

C. Surface Topology Reconstruction

To test the reconstruction method of the surface topology as presented in section III the same zick-zack profile is realised on the fluid surface using a solid PVC-block in the shape of the profile, which is pressed onto the surface at a mean surface level of 145 mm. The sensor is successively placed at the same five x-positions alongside the wide face of the vessel as in section III B. Its z-position is 130 mm. For each of these positions the calibration function is determined separately beforehand.

The result of the surface reconstruction is displayed in Figure 8 together with the prescribed shape. Just as in the simulated case (Figure 5) the surface shape is not exactly reconstructed: The overall amplitude is underestimated and the surface heights at the sides are shifted due to the averaging effect of the sensor. Nevertheless, the main features of the surface shape in form of the imprinted deflections can be extracted from the experimental reconstruction.

V. EXPERIMENTAL VALIDATION: DYNAMIC SURFACES

So far the experiments were conducted with a static fluid. In this section the sensor is used to measure transient changes of the surface position with time.

A. Setup

The experiment is conducted at the Mini-LIMMCAST facility (see Figure 9) [8]. It is used to model the continuous casting process of steel on a laboratory scale. A storage tank (tundish) on top contains GaInSn and releases it through a pipe (nozzle) into a rectangular container resembling a slab mould. The mould has the same inner dimensions as the containers used in the previous experiments and the simulation. The GaInSn flows from the bottom of the mould to a catchment tank and can be pumped back into the tundish to repeat the process.

The experiment procedure is as follows: The mould is filled up to a certain initial level with GaInSn. The experiment starts with the liquid metal flowing out of the

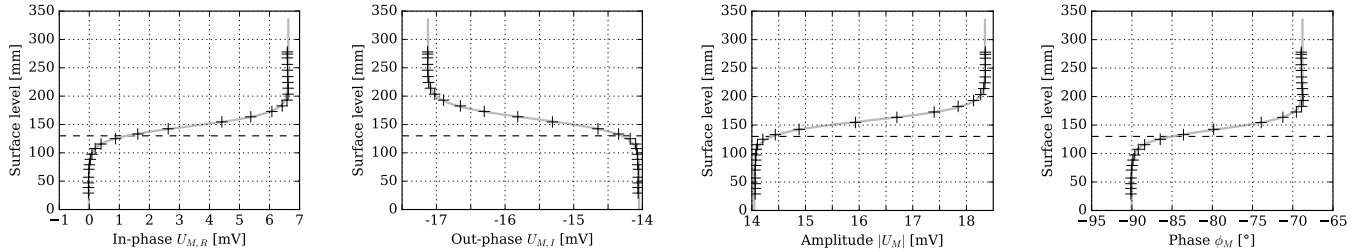

(a) (b) (c) (d)

Figure 7. Components of the measured voltage U_M for different fill heights: (a) In-phase signal $U_{M,R}$, (b) out-phase signal $U_{M,I}$, (c) amplitude $|U_M|$ and (d) phase ϕ_M. The black crosses are the measured data, the grey lines are the fits of function (5) to the data and the dashed black line shows the vertical sensor position.

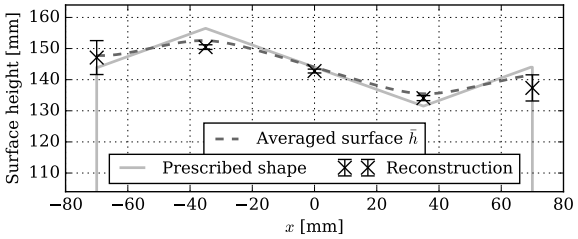

Figure 8. Result of the experimental surface topology reconstruction along the wide face of the vessel. For comparison the average surface $\bar{h}$ (8) from Figure 5 is plotted as well.

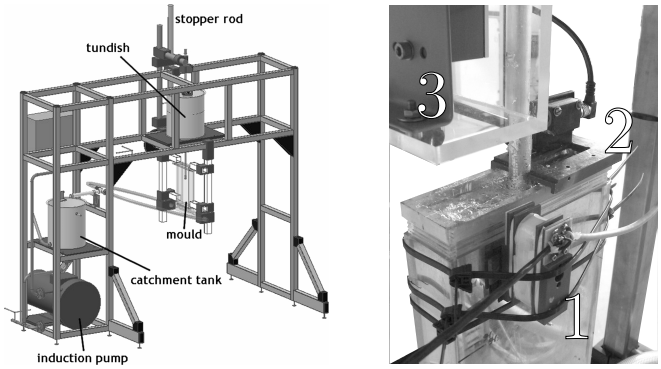

(a) (b)

Figure 9. (a) Schematic sketch of the Mini-LIMMCAST [8] and (b) photo of its mould with the different surface level measurement systems. 1: inductive, 2: ultrasonic, 3: optical.

tundish through the nozzle into the mould. The surface level rises and reaches a high position just below the brim of the mould. While the tundish empties the gravitational pressure decreases and results in a slow lowering of the surface level in the mould. Finally, when the tundish is empty, the surface level quickly drops to its initial position.

The sensor is positioned at the wide face and near the top of the mould at $z = 300\,\text{mm}$ and at $x = -35\,\text{mm}$ (Figure 9(b)) in order to avoid any influence

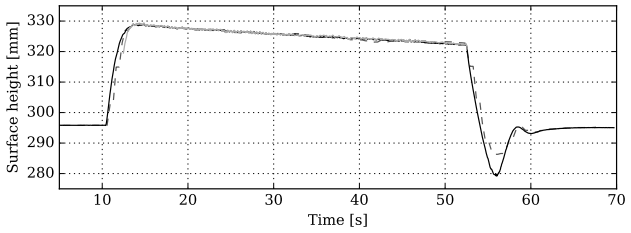

(a)

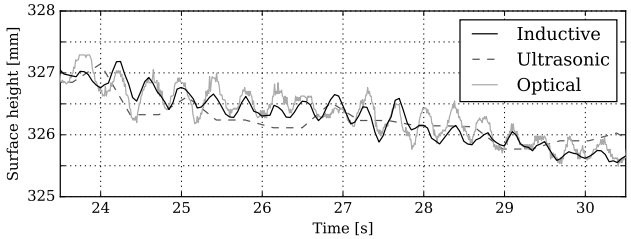

(b)

Figure 10. Transient measurement of the surface position during a Mini-LIMMCAST experiment. (a) full experiment, (b) detailed view of the surface oscillations.

of the liquid metal in the SEN during the experiment. Additionally, the surface level is measured by means of two commercial systems: an optical laser system (*MEL Laser-Scanner M2-iLan-2*) and an ultrasonic sensor (*microsonic zws-15/CI/QS*). The latter is measuring the surface position at the opposite side of the mould ($x = 35\,\text{mm}$) with a sampling frequency of 2.8 Hz and is used to calibrate the inductive sensor. The surface level is measured by the optical system at the same position as the inductive sensor with a time resolution of about 93 Hz.

B. Results

With an excitation frequency of 60 Hz and a sampling frequency of 5 kHz the inductive sensor can reach a time

resolution of 20 Hz. This value is determined by the demodulation algorithm which requires time intervals that contain a multiple of both periods, and the highest possible time resolution is the lowest common denominator of sampling and excitation frequency. Consequently, the time resolution can be improved by using different frequencies, depending on the requirements of the application.

Figure 10(a) shows the time dependent change of the surface level with time during an experiment. All measurements follow the same pattern. From the initial level of 296 mm the surface rises quickly to a position of 330 mm, slowly sinks over the duration of the experiment and returns to the initial state once the tundish is empty. Please note that the optical system cannot measure levels lower than ~ 320 mm.

During the experiment small surface oscillations were observed. In Figure 10(b) the oscillations can be found in both the laser and inductive measurement, since their time resolutions are large enough to resolve these oscillations of about 2.7 Hz (16 periods in 6 seconds). The oscillating surface cannot be reproduced by the ultrasonic sensor, since its time resolution is too small. The amplitude of the oscillations is below 1 mm peak to peak, which demonstrates the capability of the inductive sensor to resolve surface changes smaller than 1 mm.

The discrepancy between the laser and inductive measurement is below 0.5 mm. Considering that the inductive sensor is inherently an integral measurement technique, as it was discussed in section IV C, this deviation is acceptable. It justifies the assumption of a plane surface in the calibration for small surface deformations.

VI. CONCLUSION

An new inductive measurement system for determining the surface position of liquid metals was presented. It consists of individual sensors that can be combined modularly to determine the surface level at multiple near-wall positions of an arbitrarily shaped vessel. It was shown experimentally and by simulation that the main features of the surface topology can be reconstructed. A temporal resolution of 20 Hz and spatial resolution of less than 1 mm was achieved.

The next step is to conduct measurements using multiple sensors at once. Here the difficulty lies in the possibility of cross-signals between the sensors that have to be separated. Possible improvements to the measuring system include the evaluation of the measured signals, since the currently used demodulation algorithms limits the time resolution. Furthermore, an investigation of the influence of different parameters (e.g. the fluid conductivity or the excitation frequency) on the calibration could partially circumvent the need to calibrate the sensor before every use and improve the universal applicability of the system. It should be noted as well, that only non-conducting containers have been considered so far. So additionally research has to be done on the influence of e.g. copper-moulds as they are used in industrial applications.

ACKNOWLEDGMENT

This work was supported by the Helmholtz LIMTECH alliance.

[1] Micro-Epsilon Measurement, "Liquid Aluminum Level Measurement," (2016).
[2] Agellis Group AB, "EMLI," (2016).
[3] R. I. Khalilov, S. Y. Khripchenko, P. G. Frick, and R. A. Stepanov, Meas. Tech. **50**, 861 (2007).
[4] R. Moreau, *Magnetohydrodynamics* (Kluwer Academic Publishers, Dordrecht, 1990).
[5] Composition: gallium 67 % w/w, indium 20.5 % w/w, tin 12.5 % w/w.
[6] Y. Plevachuk, V. Sklyarchuk, S. Eckert, G. Gerbeth, and R. Novakovic, J. Chem. Eng. Data **59**, 757 (2014).
[7] R. H. D. Townsend, Astrophys. J. Suppl. S. **191**, 247 (2010).
[8] K. Timmel, S. Eckert, G. Gerbeth, F. Stefani, and T. Wondrak, ISIJ Int. **50**, 1134 (2010).